Journal of Photochemistry & Photobiology, B: Biology 164 (2016) 112–122

Contents lists available at ScienceDirect

Journal of Photochemistry & Photobiology, B: Biology

journal homepage: www.elsevier.com/locate/jphotobiol

Synthesis, spectroscopic, physicochemical properties and binding site analysis of 4-(1*H*-phenanthro[9,10-*d*]-imidazol-2-yl)-benzaldehyde fluorescent probe for imaging in cell biology: Experimental and theoretical study

Przemysław Krawczyk [a,*], Beata Jędrzejewska [b], Marek Pietrzak [b], Tomasz Janek [c]

[a] Nicolaus Copernicus University, Collegium Medicum, Faculty of Pharmacy, Department of Physical Chemistry, Kurpińskiego 5, 85-950 Bydgoszcz, Poland
[b] UTP University of Science and Technology, Faculty of Chemical Technology and Engineering, Seminaryjna 3, 85-326 Bydgoszcz, Poland
[c] Wroclaw Medical University, Department of Inorganic Chemistry, Faculty of Pharmacy, Borowska 211a, 50-556 Wroclaw, Poland

ARTICLE INFO

Article history:
Received 13 June 2016
Accepted 27 July 2016
Available online 19 September 2016

Keywords:
Fluorochrome
Solvatochromism
Conjugation and bioimaging
Electronic excited state
Density functional theory
AutoDock

ABSTRACT

In this study, the 4-(1*H*-phenanthro[9,10-*d*]-imidazol-2-yl)-benzaldehyde (PB1) was investigated as a fluorescent dye. For this reason, the spectroscopic properties in different solvents were thoroughly studied. The experimental data were supported by quantum-chemical calculations using density functional theory. Measurements and theoretical calculations showed that PB1 dye is characterized by the non-monotonic solvatochromism, strongly polar charge transfer excited state, large Stokes' shift, high fluorescence quantum yield and high fluorescence lifetime. Simulations using AutoDock presented in this study, showed that after conjugation with Concanavalin A in the active site with LYS116, the PB1 possesses the highest probability of binding affinity. The interaction between the PB1 dye and the Concanavalin A lectin has been investigated by circular dichroism spectroscopy. Conventional fluorescence microscopy imaging of *Candida albicans* and *Yarrowia lipolytica* cells, incubated with the PB1-Concanavalin A, was demonstrated. Results show that the PB1 dye is a photostable low molecular weight fluorescent probe, which emits a blue fluorescence. The results of this study have implications for designing PB1-protein conjugate as a valuable alternative to commercial probes designed for cellular labeling in biological and biomedical research. Calculated LogP value together with LogBCF show that PB1-protein conjugate is a valuable alternative to commercial probes designed for cellular labeling in biological and biomedical research.

1. Introduction

Achievements of recent years, the highly sensitive detection of pathogens and their reliable location inside of the human body, have contributed to the rapid and effective diagnosis and treatment of many diseases. In this field of science, the most important step is to design and synthesize suitable sensing and imaging materials that allow the correct identification of biomarkers and their quantitative determination, allowing the noninvasive and non-destructive study of biochemical processes in vivo at the cellular and molecular level [1–7]. Nowadays, the most sensitive and selective method for biological and medicinal diagnostic study is the fluorescence technology [8,9], in particular the fluorescent imaging and flow cytometry [10,11]. In vivo fluorescence imaging is the visualization of fluorescent probes as labels for molecular processes or structures. It enables a wide range of experimental measurements and monitors including the location and dynamics of gene, protein, dyes expression and molecular interactions in cells and tissues. The fluorescence signal of a fluorescence probe can be modulated and for this reason sensors relying on activation and not just accumulation, can be utilized. Moreover, dyes used herein as fluorescent probes in single or multiple analyses allow to obtain information about the cell structures and their functionality or biomarkers and physiological parameters in a more efficient and less time-consuming way [12,13]. However, the fluorescence technology is often limited due to the availability of appropriate fluorescent dyes. The fluorescent nanostructures most commonly used as fluorescent probes are: organic dyes with large delocalized π-electron systems, fluorescent proteins, metal complexes, semiconductor nanocrystals, and up conversion nanophosphors [14–17]. Among the requirements for them the most important features include: low toxicity and good solubility, high chemical and environmental stability, tolerance by living cells and deep penetration depth in living tissues, high photostability, large signal to noise ratio sharp absorption and emission under excitation, large Stokes' shift, bright fluorescence, high quantum yield and resistance to photo bleaching [18–20]. Moreover, fluorescent dyes should have a specific reactive group

* Corresponding author.
E-mail address: przemekk@cm.umk.pl (P. Krawczyk).

http://dx.doi.org/10.1016/j.jphotobiol.2016.07.044
1011-1344/

such as —CHO, —NH_2, —SH, or N-hydroxysuccinimide ester allowing an easy connection to biomolecules. Very popular are conjugate fluorescence probes with isothiocyanate group connected by covalent bonds to N-terminal amines or to amino groups on lysine side chains.

The family of imidazoles is very important due to their chemical and biological properties. Their derivatives include many substances and are an invaluable in synthesis of drugs which have broad applications in many areas of clinical medicine. Imidazoles are widely used as antiepileptic agents, antiparasitic, anthelmintic, anti-inflammatory, analgesics and platelet aggregation inhibitors [21–26] as well as antineoplastic antibiotic, muscarinic receptor antagonist, antiulcerative, prohormone, benzodiazepine antagonist, antihyperthyroid and hypnotic agents [27–30]. In this study a compound will be presented that belongs to the phenanthroimidazole class, as imidazole derivative, containing —CHO as a functional group: 4-(1*H*-phenanthro[9,10-*d*]-imidazol-2-yl)-benzaldehyde - PB1. This compound is well known in the literature as a ratiometric fluorescent probe for hydrogen sulfite [31], a ratiometric fluorescent probe for cysteine and hemocysteine [32], antimicrobial drug [33], sensitive fluorescence ratiometric probe for cyanide with its application for detection of cyanide in natural water samples and biological samples [34], solar cells [35], multifunctional agents for treatment of Alzheimer's disease [36]. In this study, the PB1 compound was prepared as imaging agents for detecting and monitoring of specific carbohydrate moieties. The experimental data are supported by quantum-chemical calculations using density functional theory (DFT) [37–43]. The DFT methods are very effective and widely used in the description and modelling of drugs and fluorescence probes and computational costs are relatively low [44–53]. Moreover, in this study was investigated the interaction of the fluorescent dye with the Concanavalin A one of the most widely used lectins in cell biology, by combining two experimental spectroscopic methods (fluorescence and circular dichroism) with molecular modelling computations.

2. Methodological Section

2.1. Experimental Part

2.1.1. Materials and Synthesis

All reagents and solvents were obtained from Aldrich Chemical Co. The 2-(4-bromophenyl)-phenanthro[9,10-*d*]imidazole was synthesized based on the procedures taken from literature [54].

The condensation of 9,10-phenanthroquinone (10 mmol) with terephtaledialdehyde (30 mmol) in the presence of ammonium acetate (50 mmol) and acetic acid (10 mL) yielded 4-(1*H*-phenanthro[9,10-*d*]-imidazol-2-yl)-benzaldehyde (Fig. 1). The reaction mixture was heated at 110 °C for 1 h under stirring, then it was cooled to room temperature. The crude product was filtered out and purified by flash chromatography [55].

$C_{22}H_{14}N_2O$; 322.35936 g/mol; mp 308.1 °C; 56.7% yield; $R_f = 0.27$ for methanol-chloroform 0.1:10 v/v.

^{1}H NMR (DMSO-d_6) δ (ppm): 7.67 (m, 2H, Ar), 7.77 (m, 2H, Ar), 8.15–8.13 (d, $J = 8.0$ Hz, 2H, Ar), 8.55–8.53 (d, $J = 8.0$ Hz, 2H, Ar), 8.59–8.57 (d, $J = 8.0$ Hz, 2H, Ar), 8.63–8.61 (d, 2H, $J = 8.0$ Hz, Ar), 8.87–8.85 (d, $J = 8.0$ Hz, 2H, Ar), 8.91–8.89 (d, $J = 8.0$ Hz, 2H, Ar), 10.11 (s, 1H, CHO), 13.73 (s, 1H, NH).

^{13}C NMR (DMSO-d_6) δ (ppm): 193.07 (CHO), 122.4, 122.7, 124.3, 124.7, 126.0, 126.3, 126.9, 127.7, 127.8, 130.6 (CH), 122.7, 127.3, 128.2, 128.8, 135.9, 136.5, 137.9, 148.2 (C).

IR (KBr) (cm^{-1}): 3197, 3084, 1690, 1604, 1567, 1455, 1425, 1296, 1216, 1171, 1039, 967, 837, 754, 723, 671, 503.

Throughout the manuscript the following notation was adopted: 1.4-Dx - 1.4-dioxane; Et_2O - diethyl ether; THF - tetrahydrofuran; MeCN - acetonitrile; DMF - *N*,*N*-dimethylformamide; DMSO - dimethylsulfoxide.

2.1.2. Measurements

The ^{1}H (400 MHz) and ^{13}C (100 MHz) NMR spectra were recorded on a Bruker Ascend™ 400 NMR spectrometers, respectively. Dimethylsulfoxide (DMSO-d_6) was used as the solvent and tetramethylsilane (TMS) as internal standard.

The IR spectra of the synthesized salts were recorded using a Bruker Vector 22 FT-IR spectrophotometer (Germany) in the range 400–4500 cm^{-1}, by KBr pellet technique.

HPLC analyses were done by Waters HPLC systems equipped with Waters 2489 UV–vis detector (detection wavelength was 370 nm), Waters 1525 Binary HPLC Pump and a Symmetry C18 column (3.5 μm, 4.6 × 75 mm). Separation was conducted under isocratic conditions with 0.8 mL/min flow rate, 25 °C, 10 μL injection volume and HPLC grade acetonitrile as a mobile phase.

Melting points were determined on the Buchi M-565 Melting Point apparatus.

Absorption and emission spectra in different polarity solvents were recorded at room temperature using a Shimadzu UV–vis Multispec-1501 spectrophotometer and a Hitachi F-4500 spectrofluorometer, respectively.

The fluorescence quantum yield of the tested compounds (ϕ) was calculated using Eq. (1):

$$\phi = \phi_{ref} \frac{IA_{ref}}{I_{ref}A} \cdot \frac{n^2}{n_{ref}^2} \quad (1)$$

where: ϕ_{ref} is the fluorescence quantum yield of the reference (Coumarin 1 in ethanol $\phi_{ref} = 0.64$ [56]) sample in ethanol, A and A_{ref} are the absorbances of the studied compound and reference sample at the excitation wavelength (404 nm), I and I_{ref} are the integrated emission intensities for the tested compounds and reference sample, n and n_{ref} are the refractive indexes of the solvents used for the compounds and the reference, respectively.

The fluorescence lifetimes were measured using an Edinburgh Instruments single-photon counting system (FLS920P Spectrometers). The excitation was provided by a picosecond diode laser generating pulses of about 55 ps at 375 nm. The compounds were studied at concentration needed to provide absorbance of 0.1 in a 10 mm cell at 375 nm. The fluorescence decays were fitted as sums of two exponentials. The average lifetime, τ_{av} was calculated as $\tau_{av} = (\Sigma_i \alpha_i \tau_i)/(\Sigma_i \alpha_i)$, where α_i and τ_i are the amplitudes and lifetimes.

2.1.3. General Protein Labeling Procedures

Concanavalin A (carbohydrate-binding protein) was conjugated with a PB1- fluorophore in phosphate-buffered saline (PBS, 10 mM phosphate, 150 mM NaCl, pH 7.4). Briefly, 2 mg of Concanavalin A was

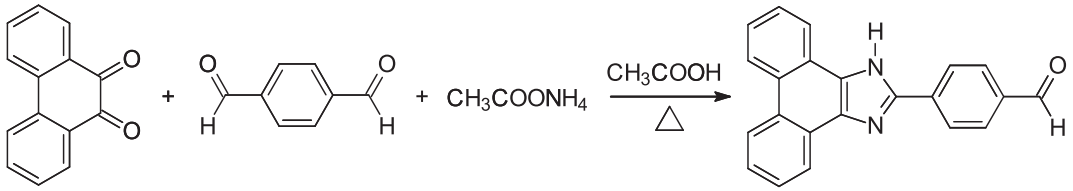

Fig. 1. A route for the synthesis of PB1 compound.

resuspended in 1 mL of buffer solution and 50 μL of 5 mg/mL PB1 in dimethylsulfoxide (DMSO) was added during vigorous mixing. The Schiff bases formed by amine-aldehyde coupling were reduced by adding 10 μL of 5 M sodium cyanoborohydride in 1 N NaOH per 1 mL reaction volume, and the reaction was allowed to proceed overnight at 4 °C. After an overnight incubation at 4 °C in the dark, unlabeled PB1 dyes were separated using a dialysis membrane centrifuge tube at 7000*g* for 10 min. The conjugated PB1-Concanavalin A solution retained in the dialysis tube was collected and diluted in PBS to a protein concentration of 1 mg/mL. The degree of labeling was determined by measuring the absorbance at 280 nm for Concanavalin A and at λ_{Abs} of the PB1 on a Varian Carry 50 Bio spectrophotometer (Varian, USA). The resultant product was stored at 4 °C.

2.1.4. Fluorescence Imaging

Candida albicans ATCC 10231 and *Yarrowia lipolytica* A101 strains were grown in a liquid yeast-peptone-glucose (YPG) medium consisting of (per liter) 10 g of yeast extract, 20 g of peptone (both from Difco), and 20 g of glucose at 28 °C with constant shaking at 200 rpm. The overnight cultures of both yeast strains were centrifuged and washed twice with PBS, pH 7.4. Then, the yeast cells were stained for 30 min at 28 °C with PB1-Concanavalin A conjugate (final concentration 0.025 mg/mL) in the PBS. Images were obtained using a Zeiss Axio Scope A1 microscope (Zeiss, Jena, Germany) with a 100× objective lens and Zeiss filter set FS01 for fluorescence microscopy. Assays were carried out three times. Representative images are presented on Fig. 2.

2.1.5. Circular Dichroism Spectroscopy

Circular dichroism spectra of 0.1 mg/mL Concanavalin A solutions were recorded on a Jasco model J-1500 spectropolarimeter (Jasco, Tokyo, Japan) at 25 °C under a constant flow of nitrogen gas, in the absence and presence of PB1 probe. The scanned wavelength domain was 190–260 nm and the time constant, scan speed, bandwidth/resolution, 50 nm/min, 2 nm and 200 millidegrees, respectively. The spectra represent the average of 9 scans. CD intensities are expressed in Δε ($dm^3/M \cdot cm$). The analysis of secondary structural contents was performed using K2D3 web server. K2D3 web server is an online tool used to assess the secondary structural elements in the form of α-helix and β-strand from the far-UV CD spectra ranging from 190 to 240 nm [57].

2.2. Computational Details

The structures of PB1 dye in its ground (S_g) and excited (S_{CT}) state were optimized by using density functional theory (DFT) approach, with the PBE0 functional [58–59] implemented in Gaussian 09 program package [60] with TIGHT threshold option. This functional was recognized as correctly describing the spectroscopic parameters in terms of experimental data for push-pull compounds [61–63] and this constituted the basis for the choice to designate the molecular structures. In order to verify that all the geometries after optimization correspond to the minima on the potential energy surface, the analysis of computed Hessian was conducted.

Using the time-dependent density functional theory (TD-DFT) [45–47] vertical transition energies and emission spectra were determined in connection with standard-hybrid PBE0 functional, as well as long range asymptotically corrected LC-ωPBE [64–66], CAM-B3LYP [67] and ωB97XD [68] functionals. The solvent effect on the linear optical properties has been taken into account using the Integral Equation Formalism for the Polarizable Continuum Model (IEF–PCM) [69–70]. In TDDFT calculations, the ground and excited states are calculated with equilibrium solvation while during considerations of the solvent effect on the fluorescence spectra the ground state should be calculated with non-equilibrium solvation [71–72]. For this reason the state-specific (SS) corrected linear response (cLR) approach [73] was employed to the theoretical calculations. In the SS approach the solvent dynamic polarizations is determined by the difference of the electron densities of the initial and final states [74–76].

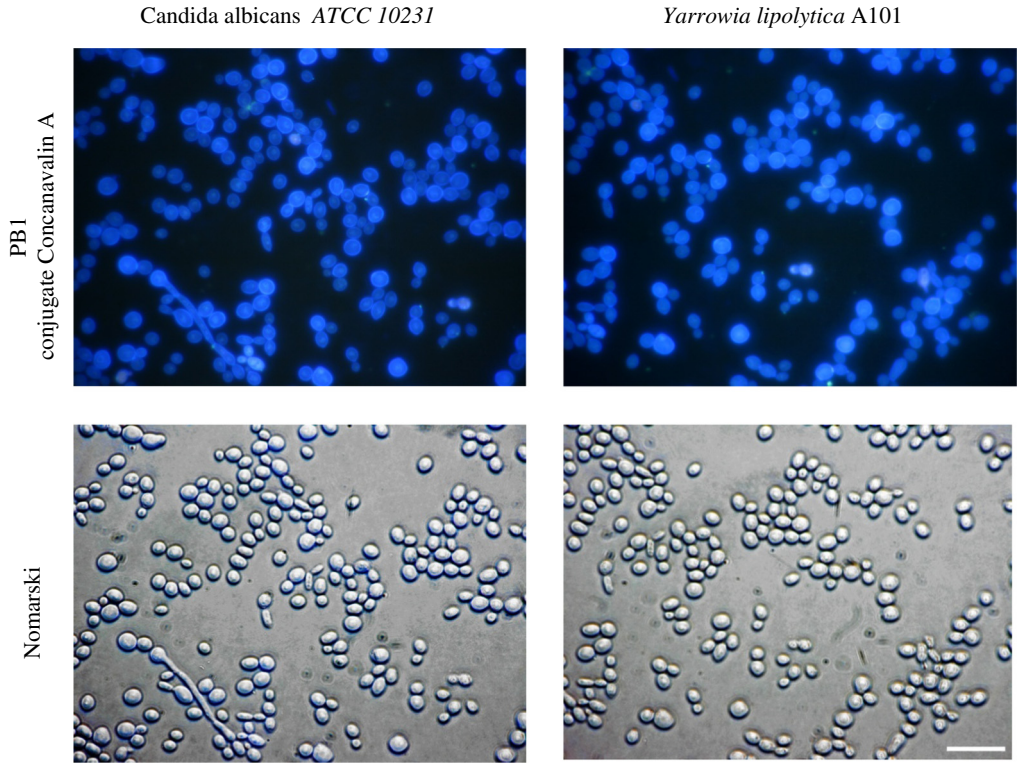

Fig. 2. Fluorescence microscope images of *Candida albicans* and *Yarrowia lipolytica* cells in the presence of dye-protein conjugate. The lectin Concanavalin A labeled with PB1 binds specifically to polysaccharides present in the cell wall of this yeast and fluoresces blue. Scale bars – 20 μm. (For interpretation of the references to color in this figure legend, the reader is referred to the web version of this article.)

The polarity of the excited state was evaluated by numerical differentiation of the excitation energies (E):

$$\Delta\mu_{ge}^{i} = \frac{E_{CT}\left(+F^{i}\right) - E_{CT}\left(-F^{i}\right)}{-2F^{i}} - \frac{E_{g}\left(+F^{i}\right) - E_{g}\left(-F^{i}\right)}{-2F^{i}} \quad (2)$$

where i states the Cartesian component of the dipole moment difference. In these calculations there was used an electric field F of 0.001 a.u. strength.

In order to identify the binding site with the highest affinity of PB1 relative to protein, the docking simulations were applied. These simulations were performed using a united-atom scoring function implemented in AutoDock Vina [77]. The preparation of the ligand and macromolecule were performed using the AutoDock Tools software package. The crystal structure of Concanavalin-A was downloaded from the Protein Data Bank in Europe (PDB ID: 2a7a) [78]. Before starting the stimulation, all the water molecules and Ca, Mg and Xe atoms were removed from the crystal structure. The conjugation of PB1 with proteins occurs via formation of a shift base between aldehyde and amino group of a lysine residue followed by reduction to a secondary or tertiary amine to give a stable alkylamine bond. For these reasons, the grid box was adjusted in such way that the space included the N-terminus of the protein and separately, in subsequent simulations, the individual —NH_2 group of lysine's side chain [79]. The docking site on protein target was defined by establishing a grid box with the dimensions of X: 14 Y: 14 Z: 14 Å, with a grid spacing of 1 Å. In simulations, the Lamarckian genetic algorithm method implemented in the AutoDock 4.2, was employed to identify appropriate binding energy and conformation of the PB1 dye. For each atom of the receptor molecule, Gasteiger charges were calculated. The docking procedure was repeated ten times for each lysine.

3. Results and Discussion

3.1. Experimental

3.1.1. Absorption and Fluorescence Spectra

Fig. 3 show the illustrative electronic absorption and the fluorescence spectra for the tested compound in selected solvents. Table 1 collects the values of the absorption and fluorescence maximum positions, molar absorption coefficients, Stokes' shifts and fluorescence quantum yields for the phenanthroimidazole derivative. The electronic absorption spectra displays a broad band with a maximum in the range from 373 to 382 nm and a high molar absorption coefficient ranging from 30,000 M^{-1} cm^{-1} to 33,000 M^{-1} cm^{-1} indicating intramolecular charge transfer (ICT) characteristics of the transition. The inspection of the data in Table 1 shows that the position of the π-π^* absorption band slightly depends on the solvent polarity. This indicates a less polar character of the PB1 in its ground state.

Table 1
The values of the absorption and fluorescence maximum positions, molar absorption coefficients, Stokes' shifts and fluorescence quantum yields for the PB1.

	λ_{max}^{Ab} [nm]	ε [M^{-1} cm^{-1}]	λ_{max}^{Fl} [nm]	ϕ_{Fl} [nm]	$\Delta\nu^{St}$ [cm^{-1}]
1,4-Dx	374.5	31,400	452.8	0.398	4617
Et_2O	373.0	33,000	439.4	0.326	4051
THF	375.5	31,400	460.2	0.544	4901
MeCN	374.5	31,300	495.2	0.696	6508
DMF	378.5	30,400	496.6	0.601	6283
DMSO	381.5	30,900	500.4	0.608	6228

As indicated in Fig. 4 and Table 1, the solvent polarity shows a significant effect on the position of fluorescence spectral maxima. The emission spectra are red-shifted by ca. 60 nm as the solvent polarity increases. This is exemplified by the increase of emission maximum from 439 nm in diethyl ether to 500 nm, observably indicating a better stabilization of the singlet excited state by polar solvents. Reasonable correlation has been found between either the fluorescence peak maxima or the Stokes' shift parameter and the solvent polarity scale, E_T^N (Fig. 4).

The substantial red shift of the emission spectra and large Stokes' shift increasing with solvents' polarity suggest different charge distribution and an increase of the dipole moment in the excited state with respect to that of the ground state.

Besides fluorescence band position also its intensity is affected by solvent polarity. As shown in Fig. 5, the fluorescence quantum yield of PB1 increases with increasing solvent polarity. The smallest value is observed in diethyl ether (ca. 33%) whereas in polar solvent, acetonitrile (MeCN), the ϕ_{Fl} equals 70%.

For the tested compound, two-exponential fluorescence decays were observed (Table 2) with one component close to 2 ns and the second about 0.3–0.6 ns. Moreover, the shortest average fluorescence lifetimes are observed in diethylether (Et_2O). The correlation between the fluorescence average lifetimes and E_T^N solvent polarity parameter for PB1 clearly demonstrates the sensitivity of its fluorescence behavior to solvents. The fluorescence lifetimes increase with an increase of solvent polarity. What is more, for PB1 the shortest fluorescence lifetime is observed for the solvent in which the fluorescence quantum yield is low, which confirms the fluorescence quenching of PB1 by specific interactions with solvent molecules.

Based on the average lifetimes and quantum yields of fluorescence data, radiative (k_r) and nonradiative (k_{nr}) rate constants have been

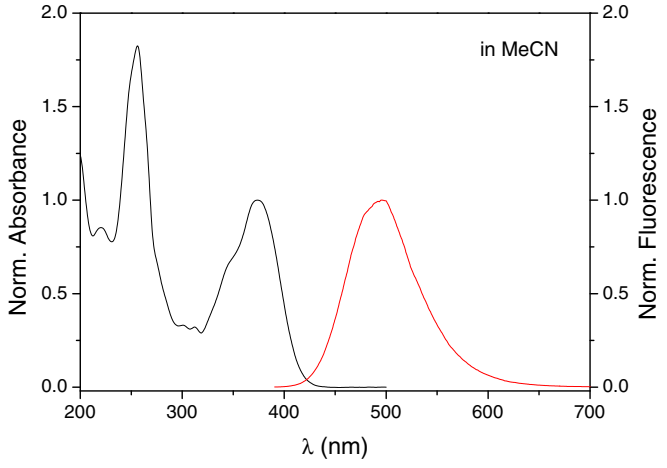

Fig. 3. Normalized electronic absorption and fluorescence spectra of PB1 in MeCN.

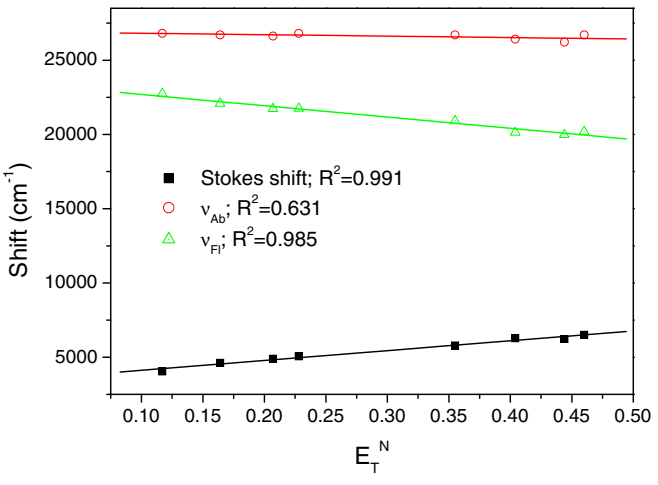

Fig. 4. Influence of solvent polarity on spectral shift for PB1 dye.

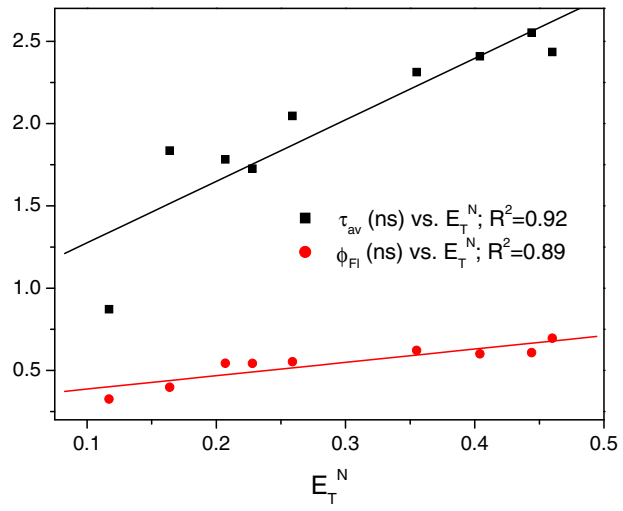

Fig. 5. Plot of fluorescence quantum yield and averaged fluorescence lifetime of tested compound versus E_T^N.

calculated according to Eqs. (3) and (4). The values are collected in Table 3.

$$k_r = \frac{\phi_{Fl}}{\tau_{av}} \tag{3}$$

$$k_{nr} = \frac{(1-\phi_{Fl})}{\tau_{av}} \tag{4}$$

Analysis of the date collected in Table 3 indicates that the k_r/k_{nr} ratio changes with solvent polarity. For PB1 compound, the k_r/k_{nr} ratio decreases suggesting a greater participation of radiative transition [80–83].

3.1.2. Synthesis of PB1-Concanavalin A Conjugates

Carbonyl groups, including aldehydes react under mild aqueous conditions with aliphatic and aromatic amines to form an intermediate known as a Schiff base (an imine), which can be selectively reduced by the mild reducing agent sodium cyanoborohydride to give a stable alkylamine bond [84]. The PB1 probes with reactive aldehyde groups were formed Schiff bases with the primary amines of Concanavalin A. The reaction efficiency and bond stability between aldehydes and primary amines was increased by the addition of sodium cyanoborohydride. The absorbance spectra of conjugates of PB1 labeled with more than 1 mol of dye per mole of protein show a pronounced increase in the shoulder about 370 nm, apparently due to interaction between the dye and the protein.

3.1.3. Protein Labeling with PB1 Fluorophore

The binding of the probes to protein has gained importance in a lot of different fields in biomedical research. This method is based on the fluorescence detection of macromolecules (such as proteins or antibodies) labeled with probes [63]. To evaluate the binding of PB1-fluorochrome to Concanavalin A in vitro, fluorescence microscopy (Fig. 2) was performed using *Candida albicans* and *Yarrowia lipolytica* cells, which were used as a positive control because Concanavalin A was used to detect the presence of carbohydrate moieties in the living yeast cells. The cell binding results indicate that the PB1-Concanavalin A conjugates accumulated selectively in yeast cells, which emits a blue fluorescence. The emission maximum of PB1 and Concanavalin A labeled with PB1 lies at about 490 nm, similar to 2-(4-amidinophenyl)-1H-indole-6-carboxamidine (DAPI) [85] and Hoechst 33,342 [86], which lie about 460 nm. For PB1-Concanavalin A conjugate dissolved in PBS, the absorption spectra is shifted by about 10–15 nm compared to PB1 in PBS. This indicates the dissociation of aggregated dye molecules in the presence of Concanavalin A. The experimental data allow us to conclude that the aggregation of PB1 in PBS is the main reason for the low fluorescence emission in aqueous solution, a process that might be reverted upon dye conjugated to the Concanavalin A, resulting in a significant fluorescence enhancement (*data not shown*). Our spectroscopic studies as well as many other literature reports reveal that there is an interplay between dye (de)aggregation and dye-protein interactions [87–88]. A similar fluorescence enhancement in the presence of proteins like amyloid β-protein has been reported for different dye including NIAD-4 [89]. The measurement protocols used for PB1 dye characterization can be exploited for dye screening, providing information on the occurrence of dye aggregation and the influence of PB1-Concanavalin A interactions on the spectroscopic properties of fluorescent reporters. Together, our data suggests that the PB1-Concanavalin A conjugates may be useful as imaging agents for detecting and monitoring of specific carbohydrate moieties [90].

Table 2
Fluorescence lifetimes of PB1 in different solvents.

	τ_1 [ns]	τ_2 [ns]	α_1	α_2	τ_{av} [ns]	χ^2
1,4-Dx	0.472	1.977	9.347	90.65	1.836	1.219
Et_2O	0.49	1.107	38.09	61.91	0.872	1.115
THF	0.612	1.965	13.43	86.57	1.783	1.299
MeCN	0.598	2.569	6.78	93.22	2.435	1.426
DMF	0.396	2.54	6.127	93.87	2.409	1.370
DMSO	0.323	2.645	3.948	96.01	2.553	1.388

Table 3
Radiative (k_r) and non-radiative (k_{nr}) rate constants for PB1 in different solvents.

	k_r (10^8 s^{-1})	k_{nr} (10^8 s^{-1})	k_r/k_{nr}
1,4-Dx	2.17	3.28	1.51
Et_2O	3.74	7.73	2.07
THF	3.05	2.56	0.84
MeCN	2.86	1.25	0.44
DMF	2.50	1.66	0.66
DMSO	2.38	1.54	0.64

3.1.4. Effects of PB1 on the Concanavalin A Secondary Structure

The circular dichroism spectrum of Concanavalin A is that of a typical lectin, with a negative band near 220 nm revealing a content of β-sheet structure [91]. Fitting the spectrum of native Concanavalin A at 25 °C yielded a 40.04% β-sheet and only 2.97% α-helical structure. The PB1-

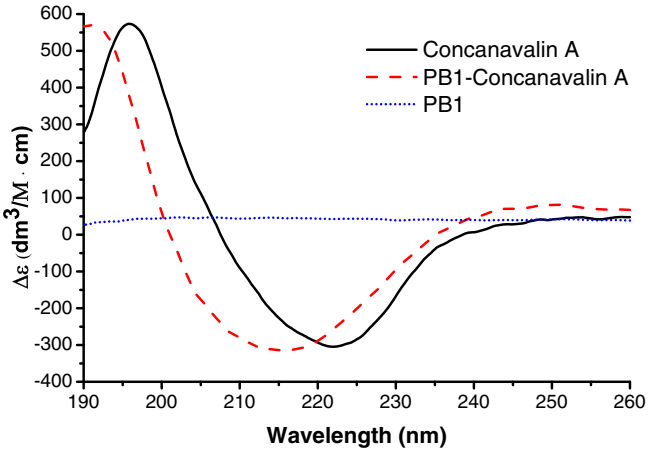

Fig. 6. Circular dichroism spectra of Concanavalin A (0.1 mg/mL) in presence of PB1 fluorochrome.

Concanavalin A conjugate caused a secondary structural change of the lectin to 24.21% β-sheet/9.54% α-helical. These spectral changes suggest the occurrence of bulk conformational modifications due to fluorophore binding to the primary amines of Concanavalin A (Fig. 6).

3.2. Theoretical Aspect

The theoretical geometric structures for the investigated compound in its ground and excited state are presented in Fig. 7. The PB1 molecule is planar, both in the ground (S_g) as well in the low-lying singlet excited state (S_{CT}). Calculated geometric parameters (see Fig. S1 and Table S1 in Supporting information) show, that torsion angles for both states are almost identical. Some differences appear only for the C12—C13—C16—H18 and C14—C13—C16—O17 torsion angles in aldehyde group, resulting in a reduced distance between the oxygen and hydrogen atoms in the excited state. Structural changes between the ground and excited state occur when the length of the bond is taken into account. Firstly, in the S_{CT} molecule the C1/C2—C16 axis seems to be slightly shorter. This is due to the observed decrease in bond lengths of C8—C10 and C13—C16 of about 0.02 Å and 0.03 Å, respectively. Moreover, C3—C4 and C5—C6 bonds in the central ring of the phenanthroimidazole are reduced while the others are lengthened. The same conclusions can be drawn from the analysis of benzene linking the aldehyde group with phenanthroimidazole. It can be noted that also the C16—O17 bond in S_{CT} is significantly lengthened (about 0.04 Å) and the C13—C16—O17 bond angle is increased which moves the oxygen atom away from the rest of the molecule. Taking into account the effect of the solvent on the structural characteristics, the polarity of the environment does not substantially influence the geometry of the ground and excited state. What it is worth mentioning, the C8—C10 bond for the S_g become longer during transitions from the vacuum to 1,4-Dx and this growth occurs with increasing polarity of the medium. However, for the S_{CT} state this bond decreases as a function of the solvent polarity. In the case of C13—C16 there is observed a reduction of bond length with the increasing dielectric permittivity of the environment while for the C16—O17 it increases, for both S_g and S_{CT}. In each case, the influence of the solvent on the S_{CT} structure is higher than on the ground state, where differences in bond lengths are almost imperceptible when changing the solvent to more polar. This dependence is reflected in the solubility of the PB1 compound, in relation to the free energy of solvation ($\Delta G_{solvation}$) [92] (see Table 4). In general, with increasing solvent polarity, the $\Delta G_{solvation}$ slightly increases. In three less polar environments this value remains almost at the same level and indicates a very good solubility of the PB 1. In the presence of water the free energy of solvation is increased by >30%. The solvation process is spontaneous and this growth significantly affects the solubility of the dye in water causing the PB1 to be very poorly soluble in this environment. Calculated solubility in water is: $2.04 \cdot 10^{-5}$ mol/L (in 25 °C, 298.15 K, 760 mm Hg).

According to the plots of frontier molecular orbitals, in the case of PB1 dye excitation to the first singlet excited state is the charge transfer (CT) excitation and is dominated by HOMO-LUMO transition (Fig. 8). The HOMO is delocalized over the entire molecule, while the LUMO is mainly localized on the benzaldehyde part and imidazole ring. The aldehyde is a moderate deactivating group but the electron-cloud mainly accumulates in this part of compound. Thus, the excited state of PB1 can be assigned as a π-π^* transition mixed with ICT process. Moreover, the value of the energy separation between HOMO-LUMO (E_{GAP}) orbitals in solvents is >3 eV (see Table S2 in Supporting information) and confirms a high fluorescent efficiency and good stability of the PKA compound [93]. On the basis of HOMO and LUMO values, the PB1 dye is characterized by a relatively low value of chemical hardness (η) and therefore should be eligible for soft molecule [94–95]. For this reason, its reactivity is very high and it undergoes uni-molecular reaction (such as with proteins) relatively quickly and easily.

A very useful tool in the designing and analysis of fluorescent probes in locating the reactive sites is the molecular electrostatic potential (MEP). The PB1 molecule has only one site for electrophilic attack (red region) which is located around the carbon atom C12 (−0.656 a.u.) (see Fig. S2) and this place can be easily protonated. Positive electrostatic potential sites are mainly localized on the middle benzene ring and in small extent on imidazole of the phenanthroimidazole reaching up to the C8—C10 bond. Therefore, the phenanthroimidazole acts as electron-donating substituent. However, the maximum positive region is

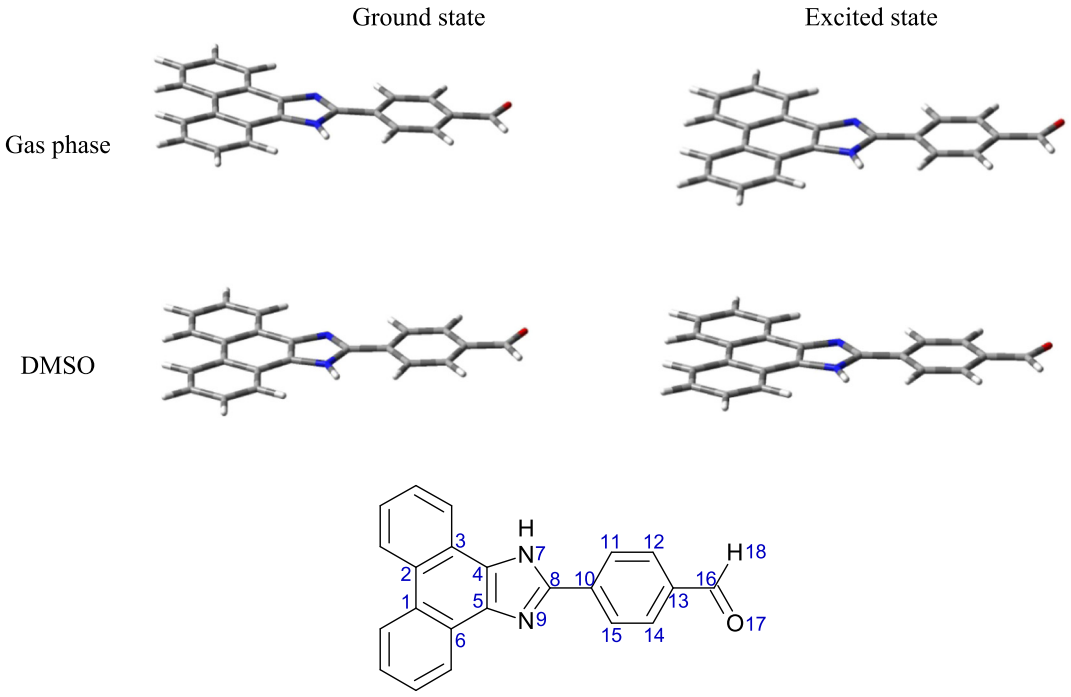

Fig. 7. Structures of the PB1 in ground and low-lying CT state in selected environments with the method of atom numbering.

Table 4
Calculated free energies of solvation in kcal/mol.

	$\Delta G_{solvation}$		
	CAM-B3LYP	LC-ωPBE	PBE0
MeCN	−24.3	−25.0	−22.7
DMF	−22.9	−23.0	−21.3
DMSO	−21.2	−21.5	−19.1
Water	−15.2	−15.6	−13.4

localized on the hydrogen atom of the nitrogen N7 (+0.862 a.u.) and this place is the most possible region for nucleophilic attack. These sites are the potential regions where the molecule can exhibit intermolecular interactions and where it can undergo non-covalent interactions.

The calculated one-photon absorption (OPA, λ^{Ab}_{calc}) maxima are presented in Tables 5, S3 and S4. Taking into account the vertical excitation energy (ΔE), values nearest to experimental ones are obtained using the standard hybrid PBE0 functional. Its application leads to a bathochromic shift of λ^{Ab}_{calc} with respect to the measured values, in average of 24 nm. In an absorption process, the solvent is in equilibrium solvation with the ground state electron density but non-equilibrium solvation with the excited state electron density. Therefore, the cLR-TDDFT calculations should give a more reasonable estimation of the transitions energies. As it is shown in Table 2, employing cLR model in connection with the PBE0, gives the λ^{Ab}_{calc} more shifted towards longer wavelengths (by over of 10 nm). More importantly, the vertical values as well as including-state-specific solvation correction indicate that the behavior of the λ^{Ab}_{calc} is non-monotonic. For molecules with positive solvatochromism a larger polarization for the CT state occurs than for the ground state. In this case, highly polar solvents cause better stabilization for the zwitterionic form and dipole moment of the CT state (μ_{CT}) is higher than for the S_g state (μ_g) [96]. When the hypsochromic shift occurs, the S_g is better stabilized by polar solvents than S_{CT} and $\mu_g > \mu_{CT}$. This blue shift could be a result of not only the solute-solvent electrostatic interaction energy between S_g and S_{CT} states of the solute but of the H-bonding interaction. As it is shown in Table S5, in each of the used solvents $\mu_g < \mu_{CT}$. Moreover, with increasing polarity of the environment, a dipole moment of the ground and CT excited state increases. The upward trend as a function of the solvent polarity also applies to the polarity of the excited state ($\Delta\mu_{g-CT} > 9$ and 13 D for the CAM-B3LYP and PBE0, respectively). This indicates that PB1 dye exhibits strongly polar charge-transfer excited state and the pure electrostatic contribution to the solute-solvent interaction should not occur. However, the short-range specific interaction cannot be excluded, e.g., hydrogen bonding which significantly affects the intensity of absorption band. The comparison of the vertical λ^{Ab}_{calc} determined theoretically with the ones obtained from experimental measurements (see Fig. S3) shows that in the region of interest they have

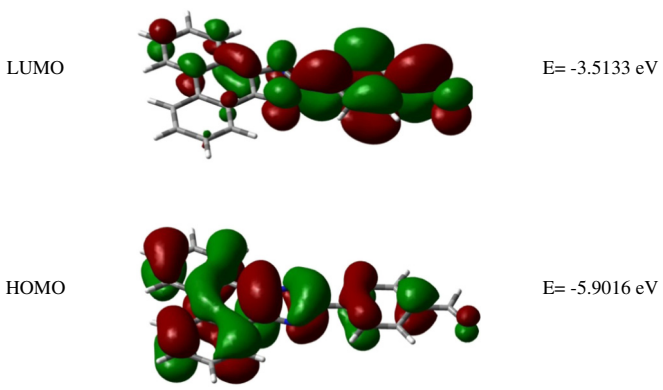

Fig. 8. The plots of frontier molecular orbitals calculated at PBE0/6-311++G(d,p).

Table 5
The vertical and state-specific corrected excitation and de-excitation energy calculated using the PBE0 functional.

	TDDFT			cLR-TDDFT	
	λ^{Ab}_{calc}	f_{os}	λ^{Fl}_{calc}	λ^{Ab}_{calc}	λ^{Fl}_{calc}
Gas phase	386.51	0.7267	421.33	–	–
1,4-Dx	399.72	0.8945	447.19	407.82	448.90
Et_2O	399.02	0.8797	446.42	409.10	476.35
THF	400.16	0.8976	470.56	412.99	491.91
MeCN	398.80	0.8841	509.41	412.32	511.79
DMF	400.48	0.9082	512.25	416.18	514.21
DMSO	400.21	0.9049	512.00	415.74	516.00
Water	398.52	0.8814	509.47	412.06	512.04

similar shapes and intensities and these intensities are unchangeable in any environment. Only near 300 nm for TD-DFT and 350 nm for experimental measurements there is an additional peak which corresponds to the n-π^* transition. In this connection it should be assumed that PB1 dye can undergo self-aggregation in medium and polar solvents which causes the solvatochromic reversal. In particular, on the MAP there are places in which the molecule can undergo not only protonation with biomolecules but also with another molecule. However, according to previously performed research [63], these observations do not substantially affect the in-vivo studies.

The theoretical fluorescence spectra (λ^{Fl}_{calc}) obtained for the PB1 dye were shown in Tables 5 and S6. Firstly, the values closest to the experimental ones are those obtained employing the PBE0 functional and $\lambda^{Fl}_{PBE0-Exp} < 15$ nm, except the 1,4-DX ($\lambda^{Fl}_{PBE0-Exp} = 23.4$ nm). The state-specific approach leads to lower values of the de-excitation energy. The inclusion of the SS correction produces a slight red shift increasing the difference between the measured and computed λ^{Fl}_{calc}. In general, it should be highlighted that differences in the $\lambda^{Fl}_{(cLR-TDDFT)-(TDDFT)}$ decrease as a function of increasing solvent polarity. However, predictability of solvatochromic behavior of the PB1 compound is similar in both cases. More importantly, the transition from the gas phase to the 1,4-Dx is accompanied by a bathochromic shift. However, as in the case of OPA, this red shift disappears as a function of the solvent polarity and the molecule is characterized by non-monotonic behavior of λ^{Fl}_{calc}. As in the case of λ^{Ab}_{calc}, the electric permittivity of the environment does not affect the intensity of λ^{Fl}_{calc} (Fig. S3) which also does not exclude the possibilities of formation H-bonds. For this reason it is difficult to speculate on the impact of solvent on position of the fluorescence maximum band, especially that the difference between DMF and water is only 3 nm and H-bond interactions are not observable in the experimental measurements. However, it must be noted that in weakly polar solvents the PB1 dye mainly tends to self-aggregate, while in strongly polar ones it is additionally quenched by specific interactions with solvent molecules.

One of the factors determining the usefulness of the dye as a fluorochrome in biomedical imaging is the Stokes' shift. For experimental measurements values of this magnitude increase with increasing polarity of the solvent in the weakly polar environments, but ranging from MeCN they slightly decrease. For theoretical calculations, $\Delta\nu^{St}$increases with increase of the dielectric permittivity. Moreover, the better similarity to the experimental data was obtained for the CAM-B3LYP functional. Its use leads to an overestimation of $\Delta\nu^{St}$ by an average of 350 cm^{-1}, while the PBE0 overestimates it by an average of >1000 cm^{-1}. On the other hand, the use of state-specific approach increases the difference in $\Delta\nu^{St}$ relative to the experimental data by 1500 $cm^{-1}$and 750 cm^{-1} for PBE0 and CAM-B3LYP respectively, but exhibits analogous non-monotonic behavior for both functionals. Therefore, it should be highlighted that the PBE0 functional is almost an universal tool in the description of spectroscopic parameters of the D-π-A systems and in an appropriate combination with other methods it is a reliable tool for theoretical modelling of fluorescent probes.

According to the literature, the conjugation of PB1 with Concanavalin A occurs via formation of a shift base between aldehyde and amino groups of a lysine residue and next by reduction to a secondary or tertiary amine to give a stable alkylamine bond. Therefore, in a protein there are several possible active sites for connecting the fluorochrome probe containing an aldehyde group. For this reason, the AutoDock simulations were employed in order to indicate the location of the site with the most likely connection of the PB1 dye with a protein. As shown in Table S7, the lowest binding free energy (ΔG_b in kcal/mol) exhibits the sites with LYS116 and calculated inhibition constant (K_i) is 0.79 mM. In other words, in this active site the PB1 dye possess the highest probability of potential binding affinity into the binding site of the Concanavalin A macromolecule. Visual inspection of this active binding site (see Fig. 9) shows that the dye is efficiently inserted into the aromatic cage framed by THR120, GLU122, VAL 187 interacting with the aromatic rings of phenanthrene part; VAL 187 interacting with imidazole part and VAL188 interacting with aromatic rings of the benzaldehyde. Also VAL 187 and LYS116 interact with this fragment of the PB1. The binding is not stabilized by the π-π stacking interaction and also the presence of H-bonds is not observed. The slightly higher value of ΔG_b characterizes the binding active site located near the LYS101. Although the $\Delta\Delta G_b$ between these sites is 0.2 kcal/mol, the K_i value is decreased to 0.49 mM. For the third binding active site (LYS30) with a relatively high affinity, the ΔG_b increases to -5.3 kcal/mol and K_i is reduced to 0.35 mM. In this bonding mode the THR3 forms the H-bond via oxygen atom with N7—H of the dye (2.798 Å) which is consistent with the MEP analysis and can affect the K_i value. Moreover, in all cases after docking the PB1 dye is twisted with respect to the reference geometry (S_g). This twisting occurs on the C8—C10 bond connecting the benzaldehyde with phenanthroimidazole part. The biggest twisting is observed when the ligand is being docked near the LYS101. In this binding mode the torsion angle N7—C8—C10—C11 is increased by 75.3°. For binding mode LYS116 with the lowest ΔG_b this angle increased only by 30.6° with respect to the S_g geometry. For the active site with LYS30 the value of the torsion angle is 62.3° but additionally the oxygen atom O17 in aldehyde is oriented in a line with hydrogen N7—H.

Fluorescent dyes require not only the characteristics of their spectroscopic properties, but also specific physicochemical features which affect the bioavailability. These properties determine both the possibility and rate of penetration through biological membranes and consequently, probability of achieving an appropriate concentration in the site of action. One of them is LogP which determines the absorption and the permeability across cell membranes. According to the Lipinski "5" rule, molecules with LogP > 5 are characterized by poor bioavailability [97]. For the PB1 dye the calculated LogP = 4.71 ± 0.36 (for QSAR calculations LogP = 4.89) which indicating a relatively good permeability trough cell membranes. The PB1 molecule is characterized by high metabolism at CYP-450 (the probability are 0.6668 and 0.9938 for the CYP450-2D6 and CYP450-3A4, respectively). In this connection it should be expected that after fulfilling its role as a fluorescent marker it should be quickly removed from the body without interacting with other drugs. The LogBCF indicates bioconcentration and refers to the process of uptake and buildup of chemicals in living organisms. For PB1 the calculated LogBCF = 3.32 which suggests that this dye will be not excreted in the urine and may be accumulate in fatty tissues [98]. On the other hand, the calculated probability of toxicity is 0.69 ± 0.1 what indicates moderate toxicity (the range 0.2–0.8). Moreover, apart from desirable characteristics for the fluorescent probes, the PB1 dye has many features which allow for its use in other areas of medical sciences and exhibits such properties as: anti-tumor, alpha- and gamma radioprotector activity and other (see Fig. S4). These calculations were performed using on-line software developed by ChemoSophia company and simulations are based on a combination of the 3D/4D QSAR BiS/MC and CoCon algorithms [99–101].

4. Conclusion

Synthesis, spectral, photophysical and some of biological properties in medium and high polar solvents of 4-(1*H*-phenanthro[9,10-*d*]-imidazol-2-yl)-benzaldehyde were described. This dye is characterized by high molar absorption coefficient and intramolecular charge transfer. The experimental measurements showed that the solvent polarity has a significant effect on the position of absorption and emission spectra and that they are characterized by positive solvatochromism. Moreover, for PB1 compound, large Stokes' shift, high fluorescence quantum yield and high fluorescence lifetime are observed which achieve their maximum

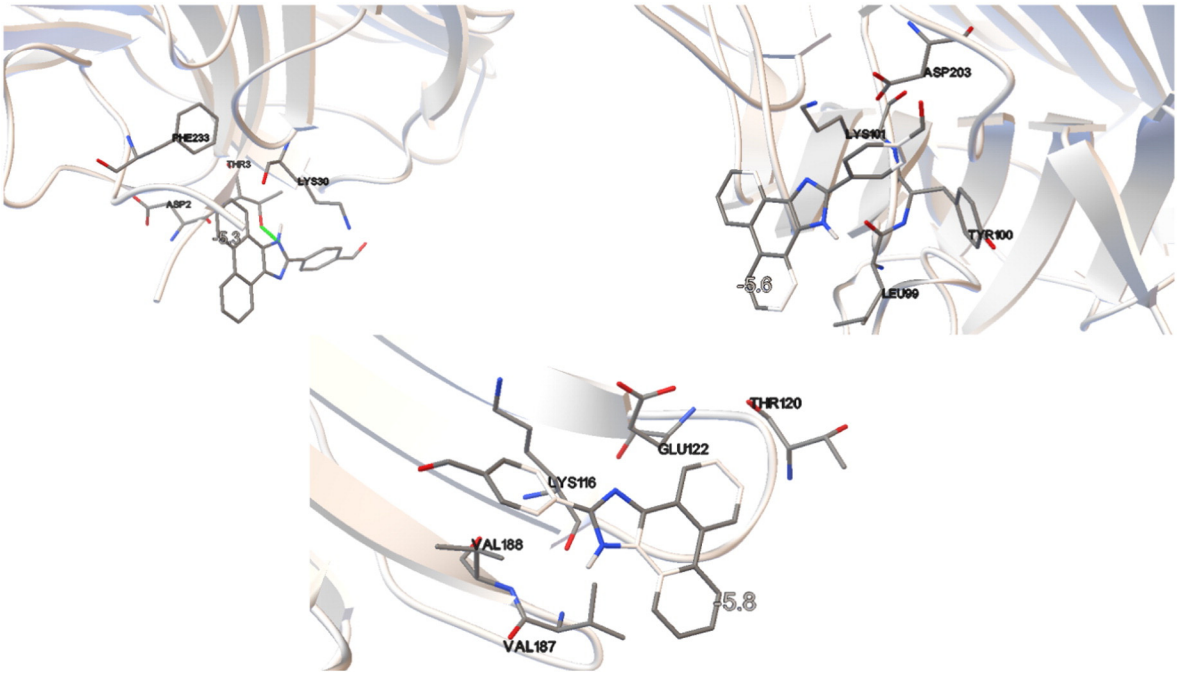

Fig. 9. Interactions between PB1 dye and active sites in the Concanavalin A.

values in polar solvents. However, the theoretical calculations clearly indicate that PB1 dye exhibits the non-monotonic solvatochromism. This dependence was revealed both in the vertical excitation energies as well as the state-specific corrected linear response approach. By contrast, the correlations of the polarity of the CT state in function of solvent polarity indicate that PB1 exhibits strongly polar charge transfer excited state and a red shift should occur. For this reason, the non-monotonic behavior should be associated with a tendency to self-aggregation in some environments which may affect solubility. The analysis of the E_{GAP} suggests a good stability, high chemical hardness and high reactivity. Simulations using AutoDock presented in this study, showed that after conjugation with Concanavalin A in the active site with LYS116 the PB1 possess the highest probability of binding affinity and in this active site there are no H-bonds interactions. One H-bond appears for active site with LYS30 which is consistent with the MEP analysis. Moreover, theoretical calculations showed a planar structure, both in the ground as well as in CT state in all solvents. Whereas, after the docking the PB1 dye undergoes twisting, which occurs on the C8—C10 bond. The usefulness of this compound in biomedical imaging was confirmed by fluorescence microscopy imaging. The in-vitro study showed that the PB1 conjugate Concanavalin A exhibited a blue fluorescence with high stability and intensity. Therefore this dye has potential applicability as a fluorescent probe and the PB1-Concanavalin A conjugates may be useful as imaging agents for detecting and monitoring of specific carbohydrate moieties. All of the properties in connection with its moderate toxicity and low LogP value show that PB1-protein conjugate is a valuable alternative to commercial probes designed for cellular labeling in biological and biomedical research.

Conflict of Interest

The authors declare that there are no conflicts of interest.

Declaration of Interest

Submitting the article “Synthesis, spectroscopic, physicochemical properties and binding site analysis of 4-(1*H*-phenanthro[9,10-d]-imidazol-2-yl)-benzaldehyde fluorescent probe for imaging in cell biology: experimental and theoretical study” to Journal of Photochemistry and Photobiology B: Biology does not have any potential conflicts of financial and non-financial interests.

Submission Declaration

Submitting the article “Synthesis, spectroscopic, physicochemical properties and binding site analysis of 4-(1*H*-phenanthro[9,10-d]-imidazol-2-yl)-benzaldehyde fluorescent probe for imaging in cell biology: experimental and theoretical study” to Journal of Photochemistry and Photobiology B: Biology has not been published previously, is not under consideration for publication elsewhere, publication is approved by all authors and it will not be published elsewhere including electronically in the same form, in English or in any other language, without the written consent of the copyright-holder.

Acknowledgements

This research was supported by the Computational Grant No. 249, PCSS (Poznan, Poland); in part by PL-Grid Infrastructure; BS 9/2014. *Yarrowia lipolytica* A101 was a kind gift of Dr. Aleksandra Mirończuk (Department of Biotechnology and Food Microbiology, Wrocław University of Environmental and Life Sciences, Wroclaw, Poland).

Appendix A. Supplementary data

Analytical data, molecular structure, photophysical properties and biological activities for investigated compound. Supplementary data associated with this article can be found in the online version, at http://dx.doi.org/10.1016/j.jphotobiol.2016.07.044.

References

[1] R. Weissleder, V. Pittet, Imaging in the era of molecular oncology, Nature 452 (2008) 580–589, http://dx.doi.org/10.1038/nature06917.
[2] L.E. Jennings, N.J. Long, ‘Two is better than one’-probes for dual-modality molecular imaging, Chem. Commun. 24 (2009) 3511–3524, http://dx.doi.org/10.1039/B821903F.
[3] J.-M. Liu, J.-T. Chen, X.-P. Yan, Near infrared fluorescent trypsin stabilized gold nanoclusters as surface plasmon enhanced energy transfer biosensor and in vivo cancer imaging bioprobe, Anal. Chem. 85 (2013) 3238–3245, http://dx.doi.org/10.1021/ac303603f.
[4] H. Guo, N.M. Idris, Y. Zhang, LRET-based biodetection of DNA release in live cells using surface-modified upconverting fluorescent nanoparticles, Langmuir 27 (2011) 2854–2860, http://dx.doi.org/10.1021/la102872v.
[5] Z. Li, Y. Zhang, S. Jiang, Multicolor core/shell-structured upconversion fluorescent nanoparticles, Adv. Mater. 20 (2008) 4765–4769, http://dx.doi.org/10.1002/adma.200801056.
[6] F. Rijke, H. Zijlmans, S. Li, T. Vail, A.K. Raap, R.S. Niedbala, H.J. Tanke, Up-converting phosphor reporters for nucleic acid microarrays, Nat. Biotechnol. 19 (2001) 273–276, http://dx.doi.org/10.1038/85734.
[7] J. Kim, H.S. Kim, N. Lee, T. Kim, H. Kim, T. Yu, I.C. Song, W.K. Moon, T. Hyeon, Multifunctional uniform nanoparticles composed of a magnetite nanocrystal core and a mesoporous silica shell for magnetic resonance and fluorescence imaging and for drug delivery, Angew. Chem. Int. Ed. Eng. 47 (2008) 8438–8441, http://dx.doi.org/10.1002/anie.200802469.
[8] P. Mitra, M. Banerjee, S. Biswas, S. Basu, Protein interactions of merocyanine 540: spectroscopic and crystallographic studies with lysozyme as a model protein, J. Photochem. Photobiol. B 121 (2013) 46–56, http://dx.doi.org/10.1016/j.jphotobiol.2013.02.010.
[9] N. Romanov, C. Anastasi, X. Liu, Cyanine Dyes for Labeling Molecular Ligands With Improved Fluorescence Intensity and Photostability, 2013 (WO2013041117 A1).
[10] M. Fernández-Suárez, A.Y. Ting, Fluorescent probes for super-resolution imaging in living cells, Nat. Rev. Mol. Cell Biol. 9 (2008) 929–943, http://dx.doi.org/10.1038/nrm2531.
[11] C. Basford, N. Forraz, C. McGuckin, Optimized multiparametric immunophenotyping of umbilical cord blood cells by flow cytometry, Nat. Protoc. 5 (2010) 1337–1346, http://dx.doi.org/10.1038/nprot.2010.88.
[12] S. Lindström, Flow cytometry and microscopy as means of studying single cells: a short introductional overview, Methods Mol. Biol. 853 (2012) 13–15, http://dx.doi.org/10.1007/978-1-61779-567-1_2.
[13] M. Díaz, M. Herrero, L.A. Garcia, C. Quirós, Application of flow cytometry to industrial microbial bioprocesses, Biochem. Eng. J. 48 (2010) 385–407, http://dx.doi.org/10.1016/j.bej.2009.07.013.
[14] L. Wang, X. Zhu, C. Xie, N. Ding, X. Weng, W. Lu, X. Wei, C. Li, Imaging acidosis in tumors using a pH-activated near-infrared fluorescence probe, Chem. Commun. 48 (2012) 11677–11679, http://dx.doi.org/10.1039/C2CC36488C.
[15] K. Li, B. Liu, Polymer encapsulated conjugated polymer nanoparticles for fluorescence bioimaging, J. Mater. Chem. 22 (2012) 1257–1264, http://dx.doi.org/10.1039/C1JM14397B.
[16] S. Zeng, M.-K. Tsang, C.-F. Chan, K.-L. Wong, J. Hao, PEG modifiedBaGdF$_5$: Yb/Er nanoprobes for multi-modal upconversion fluo-rescent, in vivo X-ray computed tomography and biomagnetic imaging, Biomaterials 33 (2012) 9232–9238, http://dx.doi.org/10.1016/j.biomaterials.2012.09.019.
[17] T. Yang, Q. Liu, S. Pu, Z. Dong, C. Huang, F. Li, Fluorophore-photochrome co-embedded polymer nanoparticles for photoswitchable fluorescence bioimaging, Nano Res. 5 (2012) 494–503, http://dx.doi.org/10.1007/s12274-012-0235-0.
[18] D. Janczewski, Y. Zhang, G.K. Das, D.K. Yi, P. Padmanabhan, K.K. Bhakoo, T.T. Tan, S.T. Selvan, Bimodal magnetic-fluorescent probes forbioimaging, Microsc. Res. Tech. 74 (2011) 563–576, http://dx.doi.org/10.1002/jemt.20912.
[19] M. Tsuji, S. Ueda, T. Hirayama, K. Okuda, Y. Sakaguchi, A. Isono, H. Nagasawa, FRET-based imaging of transbilayer movement of pepducin in living cells by novel intracellular bioreductively activatable fluorescent probes, Org. Biomol. Chem. 11 (18) (2013) 3030–3037, http://dx.doi.org/10.1039/C3OB27445D.
[20] F. Auzel, Upconversion and anti-stokes processes with f and d ions in solids, Chem. Rev. 104 (1) (2004) 139–174, http://dx.doi.org/10.1021/cr020357g.
[21] U. Uçucu, N.G. Karaburun, I. Işikdağ, Synthesis and analgesic activity of some 1-benzyl-2-substituted-4,5-diphenyl-1H-imidazole derivatives, Farmaco 56 (2001) 285–290, http://dx.doi.org/10.1016/S0014-827X(01)01076-X.
[22] A. Yeşilada, S. Koyunoğlu, N. Saygili, E. Kupeli, E. Yeşilada, E. Bedir, I. Khanc, Synthesis, anti-inflammatory and analgesic activity screening of some new 4-(3H)-quinazolinone derivatives, Arch. Pharm. Pharm. Med. Chem. 337 (2004) 96–104, http://dx.doi.org/10.1002/ardp.200200752.
[23] L. Quattara, M. Debaert, R. Cavier, Synthesis and antiparasitic activity of new nitro-5-imidazole derivatives, Farmaco. (Sci) 42 (6) (1987) 449–456 (PMID:2904887).
[24] S. Dutta, Synthesis and anthelmintic activity of some novel 2-substituted-4,5-diphenyl imidazoles, Acta Pharma. 60 (2) (2010) 229–235, http://dx.doi.org/10.2478/v10007-010-0011-1.
[25] A.K. Sengupta, T. Bhattacharya, Synthesis and antimicrobial activity of some substituted 2-phenyl-3-arylquinazol-4-ones, J. Indian Chem. Soc. 60 (1983) 373–376, http://dx.doi.org/10.1002/chin.198349246.
[26] L. Navidpour, H. Shadnia, H. Shafaroodi, M. Amini, R. Dehpour, A. Shafiee, Design, synthesis and biological evaluation of substituted 2-alkylthio-1,5-diarylimidazoles

as selective COX-2 inhibitors, Bioorg. Med. Chem. 15 (2007) 1976–1982, http://dx.doi.org/10.1016/j.bmc.2006.12.041.
[27] G. Fluoret, Synthesis of pyroglutamylhistidylprolineamide by classical and solid phase methods, J. Med. Chem. 13 (1970) 843–845, http://dx.doi.org/10.1021/jm00299a011.
[28] R.N. Brogden, R.C. Heel, T.M. Speight, G.S. Avery, Metronidazole in anaerobic infections: a review of its activity, pharmacokinetics and therapeutic use, Drugs 16 (5) (1978) 387–417 (PMID:363399).
[29] R.W. Brimblecombe, W.A.M. Duncan, G.J. Durant, J.C. Emmett, C.R. Ganellin, M.E. Parsons, J.W. Black, The pharmacology of cimetidine, a new histamine H_2-receptor antagonist, J. Int. Med. Res. 3(2) (1975) 86–92, Br. J. Pharmacol. 53 (1975) 435–436, http://dx.doi.org/10.1111/j.1476-5381.2010.00854.x.
[30] W. Hunkeler, H. Möhler, L. Pieri, P. Polc, E.P. Bonetti, R. Cumin, R. Schaffner, W. Haefely, Selective antagonists of benzodiazepines, Nature 290 (1981) 514–516, http://dx.doi.org/10.1038/290514a0.
[31] X. Cheng, H. Jia, J. Feng, J. Qin, Z. Li, "Reactive" probe for hydrogen sulfite: good ratiometric response and bioimaging application, Sensors Actuators B 184 (2013) 274–280, http://dx.doi.org/10.1016/j.snb.2013.04.070.
[32] W. Lin, L. Long, L. Yuan, Z. Cao, B. Chen, W. Tan, A ratiometric fluorescent probe for cysteine and homocysteine displaying a large emission shift, Org. Lett. 10 (24) (2008) 5577–5580, http://dx.doi.org/10.1021/ol802436j.
[33] Jawaharmal, H.S. Lamba, S. Narwal, G. Singh, D.R. Saini, A. Kaur, S. Narwal, Synthesis of novel imidazole compounds and evaluation of their antimicrobial activity, Indo Global J. Pharm. Sci. 2 (2) (2012) 147–156 (ISSN 2249-1023).
[34] L. Long, L. Zhou, L. Wang, S. Meng, A. Gong, F. Du, C. Zhang, A highly selective and sensitive fluorescence ratiometric probe for cyanide and its application for detection of cyanide in natural water sample and biological sample, Anal. Methods 5 (2013) 6605–6610, http://dx.doi.org/10.1039/C3AY41475B.
[35] M.-S. Tsai, Y.-C. Hsu, J.T. Lin, H.-C. Chen, C.-P. Hsu, Organic dyes containing 1H-phenanthro[9,10-*d*]imidazole conjugation for solar cells, J. Phys. Chem. C 111 (50) (2007) 18785–18793, http://dx.doi.org/10.1021/jp075653h.
[36] J. Liu, J. Qiu, M. Wang, L. Wang, L. Su, J. Gao, Q. at all, synthesis and characterization of 1H-phenanthro[9,10-*d*]imidazole derivatives as multifunctional agents for treatment of Alzheimer's disease, Biochim. Biophys. Acta 1840 (9) (2014) 2886–2903, http://dx.doi.org/10.1016/j.bbagen.2014.05.005.
[37] P. Hohenberg, W. Kohn, Inhomogeneous electron gas, Phys. Rev. 136 (1964) B864–B871, http://dx.doi.org/10.1103/physrev.136.b864.
[38] W. Kohn, L.J. Sham, Self-consistent equations including exchange and correlation effects, Phys. Rev. 140 (1965) A1133–A1138, http://dx.doi.org/10.1103/physrev.140.a113.
[39] R.G. Parr, W. Yang, Density-functional Theory of Atoms and Molecules, Oxford Univ. Press, Oxford, 1989.
[40] Ed.D.R. Salahub, M.C. Zerner, The Challenge of d and f Electrons, ACS, Washington DC, 1989.
[41] C. Sosa, C. Lee, Density-functional description of transition structures using nonlocal corrections. Silylene insertion reactions into the hydrogen molecule, J. Chem. Phys. 98 (1993) 8004–8011, http://dx.doi.org/10.1063/1.464554.
[42] G.E. Scuseria, Comparison of coupled-cluster results with a hybrid of Hartree-Fock and density functional theory, J. Chem. Phys. 97 (1992) 7528–7530, http://dx.doi.org/10.1063/1.463977.
[43] Ed.J.K. Labanowski, J.W. Andzelm, Density Functional Methods in Chemistry, Springer-Verlag, New York, 1991.
[44] M. Kurt, T.R. Sertbakan, M. Ozduran, An experimental and theoretical study of molecular structure and vibrational spectra of 3- and 4-pyridineboronic acid molecules by density functional theory calculations, Spectrochim. Acta A 70 (3) (2008) 664–673, http://dx.doi.org/10.1016/j.saa.2007.08.019.
[45] C. Adamo, G.E. Scuseria, V. Barone, Accurate excitation energies from time-dependent density functional theory: assessing the PBE0 model, J. Chem. Phys. 111 (1999) 2889–2899, http://dx.doi.org/10.1063/1.479571.
[46] C.J. Jamorski-Jödicke, H.P. Lüthi, Time-dependent density-functional theory investigation of the formation of the charge transfer excited state for a series of aromatic donor–acceptor part I, J. Chem. Phys. 117 (2002) 4146–4156, http://dx.doi.org/10.1063/1.1498817.
[47] V. Cavillot, B. Champagne, Time-dependent density functional theory simulation of UV/visible absorption spectra of zirconocene catalysts, Chem. Phys. Lett. 354 (2002) 449–457, http://dx.doi.org/10.1016/S0009-2614(02)00161-6.
[48] C. Ravikumar, I.H. Joe, V.S. Jayakumar, Charge transfer interactions and nonlinear optical properties of push–pull chromophore benzaldehyde phenylhydrazone: a vibrational approach, Chem. Phys. Lett. 460 (2008) 552–558, http://dx.doi.org/10.1016/j.cplett.2008.06.047.
[49] R. Zhang, B. Du, G. Sun, Y. Sun, Experimental and theoretical studies on o-, m- and p-chlorobenzylideneaminoantipyrines, Spectrochim. Acta A 75 (2010) 1115–1124, http://dx.doi.org/10.1016/j.saa.2009.12.067.
[50] F.J.A. Ferrer, F. Santoro, R. Improta, The excited state behavior of cytosine in the gas phase: a TD-DFT study, Comp. Theor. Chem. 1040–1041 (2014) 186–194, http://dx.doi.org/10.1016/j.comptc.2014.03.010.
[51] N. Sekar, P.G. Umape, V.S. Padalkar, R.P. Tayade, P. Ramasami, Synthesis of novel styryl derivatives from 4-chloro-2-(morpholin-4-yl)-1,3-thiazole-5-carbaldehyde, study of their photophysical properties and DFT computations, J. Lumin. 150 (2014) 8–18, http://dx.doi.org/10.1016/j.jlumin.2014.01.060.
[52] H. Wang, J. Shi, et al., Synthesis and characteristics of novel fluorescence dyes based on chromeno[4,3,2-*de*][1,6]naphthyridine framework, Spectrochim. Acta A 103 (2013) 62–67, http://dx.doi.org/10.1016/j.saa.2012.10.075.
[53] H. Wang, L.F. Chen, et al., Spectral studies of multi-branched fluorescence dyes based on triphenylpyridine core, Spectrochim. Acta A 121 (121) (2014) 355–362, http://dx.doi.org/10.1016/j.saa.2013.10.087.
[54] R. Francke, R.D. Little, Optimizing electron transfer mediators based on arylimidazoles by ring fusion: synthesis, electrochemistry, and computational analysis of 2-aryl-1-methylphenanthro[9,10-*d*]imidazoles, JACS 136 (1) (2014) 427–435, http://dx.doi.org/10.1021/ja410865z.
[55] W. Lin, L. Long, B. Chen, W. Tan, A ratiometric fluorescent probe for hypochlorite based on a deoximation reaction, Chem. Eur. J. 15 (2009) 2305–2309, http://dx.doi.org/10.1002/chem.200802054.
[56] J. Olmsted III, Calorimetric determinations of absolute fluorescence quantum yields, J. Phys. Chem. 83 (20) (1979) 2557–2682, http://dx.doi.org/10.1021/j100483a006.
[57] C. Louis-Jeune, M.A. Andrade-Navarro, C. Perez-Iratxeta, Prediction of protein secondary structure from circular dichroism using theoretically derived spectra, Proteins 80 (2) (2011) 374–381, http://dx.doi.org/10.1002/prot.23188.
[58] J.P. Perdew, K. Burke, M. Ernzerhof, Generalized gradient approximation made simple, Phys. Rev. Lett. 77 (1996) 3865–3868, http://dx.doi.org/10.1103/PhysRevLett.77.3865.
[59] J.P. Perdew, K. Burke, M. Ernzerhof, Errata: generalized gradient approximation made simple, Phys. Rev. Lett. 78 (1997) 1396, http://dx.doi.org/10.1103/PhysRevLett.78.1396.
[60] M.J. Frisch, G.W. Trucks, G.B. Schlegel, et al., Gaussian 09, Revision A.1, Gaussian, Inc., Wallingford CT, 2009.
[61] B. Jędrzejewska, P. Krawczyk, M. Gordel, M. Samoć, Synthesis and photophysical properties of two-photon chromophores containing 1H-benzimidazole residue, Dyes Pigments 162 (2014) 162–175, http://dx.doi.org/10.1016/j.dyepig.2014.06.007.
[62] P. Krawczyk, Time-dependent density functional theory calculations of the solvatochromism of some azo sulfonamide fluorochromes, J. Mol. Model. 21 (2015) 118–136, http://dx.doi.org/10.1007/s00894-015-2651-z.
[63] P. Krawczyk, M. Pietrzak, T. Janek, B. Jędrzejewska, P. Cysewski, Spectroscopic and nonlinear optical properties of new chalcone fluorescent probes for bioimaging applications: theoretical and experimental study, J. Mol. Model. 22 (2016) 125, http://dx.doi.org/10.1007/s00894-016-2990-4.
[64] H. Iikura, T. Tsuneda, T. Yanai, K. Hirao, Long-range correction scheme for generalized-gradient-approximation exchange functionals, J. Chem. Phys. 115 (2001) 3540–3544, http://dx.doi.org/10.1063/1.1383587.
[65] O.A. Vydrov, G.E. Scuseria, Assessment of a long range corrected hybrid functional, J. Chem. Phys. 125 (2006), 234109-9http://dx.doi.org/10.1063/1.2409292.
[66] O.A. Vydrov, G.E. Scuseria, J.P. Perdew, Tests of functionals for systems with fractional electron number, J. Chem. Phys. 126 (2007), 1541009-9http://dx.doi.org/10.1063/1.2723119.
[67] T. Yanai, D.P. Tew, N.C. Handy, A new hybrid exchange-correlation functional using the Coulomb-attenuating method (CAM-B3LYP), Chem. Phys. Lett. 393 (2004) 51–57, http://dx.doi.org/10.1016/j.cplett.2004.06.011.
[68] J.D. Chai, M. Head-Gordon, Long-range corrected hybrid density functionals with damped atom-atom dispersion corrections, Phys. Chem. Chem. Phys. 10 (2008) 6615–6620, http://dx.doi.org/10.1039/B810189B.
[69] M.T. Cancés, B. Mennucci, J. Tomasi, A new integral equation formalism for the polarizable continuum model: theoretical background and applications to isotropic and anisotropic dielectrics, J. Chem. Phys. 107 (1997) 3032, http://dx.doi.org/10.1063/1.474659.
[70] M. Arivazhagan, P. Muniappan, R. Meenakshi, G. Rajavel, PCM/TD-DFT analysis of 1-bromo-2,3-dichlorobenzene – a combined study of experimental (FT-IR and FT-Raman) and theoretical calculations, Spectrochim. Acta A 105 (2013) 497–508, http://dx.doi.org/10.1016/j.saa.2012.11.033.
[71] N. Minezawa, State-specific solvation effect on the intramolecular charge transfer reaction in solution: a linear-response free energy TDDFT method, Chem. Phys. Lett. 608 (2014) 140–144 (DOI: j.cplett.2014.05.104).
[72] G.S. Ming Tong, K.T. Chan, X. Chang, Ch.-M. Che, Theoretical studies on the photophysical properties of luminescent pincer gold(III) arylacetylide complexes: the role of p-conjugation at the C-deprotonated [C^N^C] ligand, Chem. Sci. 6 (2015) 3026–3037, http://dx.doi.org/10.1039/c4sc03697b.
[73] C. Guido, S. Caprasecca, Corrected Linear Response, State-specific Correction to Solvent Polarization Response, 2016 https://www1.dcci.unipi.it/molecolab/tools/white-papers/pisalr/; http://dx.doi.org/10.13140/RG.2.1.1903.7845.
[74] L.V. SlipchenkO, Solvation of the excited states of chromophores in polarizable environment: orbital relaxation versus polarization, J. Phys. Chem. A 114 (2010) 8824–8830, http://dx.doi.org/10.1021/jp101797a.
[75] K. Sneskov, T. Schwabe, O. Christiansen, J. Kongsted, Scrutinizing the effects of polarization in QM/MM excited state calculations, Phys. Chem. Chem. Phys. 13 (2011) 18551–18560, http://dx.doi.org/10.1039/C1CP22067E.
[76] M. Caricato, A comparison between state-specific and linear-response formalisms for the calculation of vertical electronic transition energy in solution with the CCSD-PCM method, J. Chem. Phys. 139 (2013) 044116, http://dx.doi.org/10.1063/1.4816482.
[77] O. Trott, A.J. Olson, AutoDock Vina: improving the speed and accuracy of docking with a new scoring function, efficient optimization and multithreading, J. Comput. Chem. 31 (2010) 455–461, http://dx.doi.org/10.1002/jcc.21334.
[78] C. Mueller-Dieckmann, S. Panjikar, P.A. Tucker, M.S. Weiss, On the routine use of soft X-rays in macromolecular crystallography. Part III. The optimal data-collection wavelength, Acta Crystallogr. D Biol. Crystallogr. 61 (2005) 1263–1272, http://dx.doi.org/10.2210/pdb2a7e/pdb.
[79] N. Jentof, D.G. Dearborn, Labeling of proteins by reductive methylation using sodium cyanoborohydride, J. Biol. Chem. 254 (11) (1979) 4359–4365 (PMID:571437).
[80] M. Shaikh, J. Mohanty, P.K. Singh, A.C. Bhasikuttan, R.N. Rajule, V.S. Satam, S.R. Bendre, V.R. Kanetkar, H. Pal, Contrasting solvent polarity effect on the photophysical properties of two newly synthesized aminostyryl dyes in the

lower and in the higher solvent polarity regions, J. Phys. Chem. A 114 (2010) 4507–4519, http://dx.doi.org/10.1021/jp9107969.
[81] T. Shim, M.H. Le, D. Kim, Y. Ouchi, Comparison of photophysical properties of the hemicyanine dyes in ionic and nonionic solvents, J. Phys. Chem. B 112 (7) (2008) 1906–1912, http://dx.doi.org/10.1021/jp076757v.
[82] J.B. Birks, Organic Molecular Photophysics, John Wiley and Sons, New York, 1973.
[83] S.A. El-Daly, A.M. Asiri, S.A. Khan, K.A. Alamry, Spectral properties and micellization of 1-(2,5-dimethyl-thiophene-3-yl)-3-(2,4,5-trimethoxy-phenyl)-propenone(DTTP) in different media, J. Lumin. 134 (2013) 819–824, http://dx.doi.org/10.1016/j.jlumin.2012.06.043.
[84] M. Brinkley, A brief survey of methods for preparing protein conjugates with dyes, haptens, and cross-linking reagents, Bioconjug. Chem. 3 (1) (1992) 2–13, http://dx.doi.org/10.1021/bc00013a001.
[85] J. Kapuscinski, DAPI: a DNA-specific fluorescent probe, Biotech. Histochem. 70 (5) (1995) 220–233, http://dx.doi.org/10.3109/10520299509108199.
[86] T. Janek, A. Krasowska, A. Radwanska, M. Lukaszewicz, Lipopeptide biosurfactant pseudofactin II induced apoptosis of melanoma A 375 cells by specific interaction with the plasma membrane, PLoS One 8 (3) (2013), e57991http://dx.doi.org/10.1371/journal.pone.0057991.
[87] M. Grabolle, J. Pauli, R. Brehm, U. Resch-Genger, Structural control of dye–protein binding, aggregation and hydrophilicity in a series of asymmetric cyanines, Dyes Pigments 103 (2014) 118–126, http://dx.doi.org/10.1016/j.dyepig.2013.11.027.
[88] A.S. Tatikolov, Polymethine dyes as spectral-fluorescent probes for biomacromolecules, J. Photochem. Photobiol. C 13 (2012) 55–90, http://dx.doi.org/10.1016/j.jphotochemrev.2011.11.001.
[89] F. Peccati, J. Hernando, L. Blancafort, X. Solans-Monfort, M. Sodupe, Disaggregation-induced fluorescence enhancement of NIAD-4 for the optical imaging of amyloid-β fibrils, PCCP 17 (2015) 19718–19725, http://dx.doi.org/10.1039/c5cp02728d.
[90] M.D. Disney, J. Zheng, T.M. Swager, P.H. Seeberger, Detection of bacteria with carbohydrate-functionalized fluorescent polymers, J. Am. Chem. Soc. 126 (41) (2004) 13343–13346, http://dx.doi.org/10.1021/ja047936i.
[91] S.W. Provencher, J. Glockner, Estimation of globular protein secondary structure from circular dichroism, Biochemistry 20 (1) (1981) 33–37, http://dx.doi.org/10.1021/bi00504a006.
[92] A. Kaczmarek – Kędziera, M. Ziegler – Borowska, D. Kędziera, Chemia obliczeniowa w laboratorium organicznym, Wydawnictwo UMK, Toruń, 2014.
[93] R.V. Solomon, R. Jagadeesan, S.A. Vedha, P. Venuvanalingam, A DFT/TDDFT modeling of bithiophene azo chromophores for optoelectronic applications, Dyes Pigments 100 (2014) 261–268, http://dx.doi.org/10.1016/j.dyepig.2013.09.016.
[94] R.G. Pearson, Hard and soft acids and bases, J. Am. Chem. Soc. 85 (1963) 3533–3539, http://dx.doi.org/10.1021/ja00905a001.
[95] V.K. Jain, Ab initio theoretical reinvestigation of the ground and excited state properties of silylated coumarins: good candidates for solid state dye laser and dye-sensitized solar cells, Spectrochim. Acta A Mol. Biomol. Spectrosc. 150 (2015) 806–813, http://dx.doi.org/10.1016/j.saa.2015.06.034.
[96] W. Bartkowiak, Solvatochromism and nonlinear optical properties of donor-acceptor π-conjugated molecules, in: M.G. Papadopoulos, A.J. Sadlej, J. Leszczynski (Eds.), Non-linear Optical Properties of Matter; From Molecules to Condensed Phases, Springer, Berlin 2006, pp. 299–318.
[97] Ch. Lipinski, F. Lombardo, B.W. Dominy, P.J. Feeney, Experimental and computational approaches to estimate solubility and permeability in drug discovery and development setting, Adv. Drug Deliv. Rev. 23 (1997) 3–25, http://dx.doi.org/10.1016/S0169-409X(00)00129-0.
[98] S.L. Klosterhaus, R. Grace, M.C. Hamilton, D. YeE, Method validation and reconnaissance of pharmaceuticals, personal care products, and alkylphenols in surface waters, sediments, and mussels in an urban estuary, Environ. Int. 54 (2013) 92–99, http://dx.doi.org/10.1016/j.envint.2013.01.009.
[99] V. Potemkin, M. Grishina, Principles for 3D/4D QSAR classification of drugs, Drug Discov. Today 13 (21–22) (2008) 952–959, http://dx.doi.org/10.1016/j.drudis.2008.07.006.
[100] V. Potemkin, M. Grishina, A new paradigm for pattern recognition of drugs, J. Comput. Aided Mol. Des. 22 (6–7) (2008) 489–505, http://dx.doi.org/10.1007/s10822-008-9203-x.
[101] V.A. Potemkin, A.A. Pogrebnoy, M.A. Grishina, Technique for energy decomposition in the study of “receptor-ligand” complexes, J. Chem. Inf. Model. 49 (6) (2009) 1389–1406, http://dx.doi.org/10.1021/ci800405n.